Dalton Transactions

Switching On Single-Molecule Magnet Properties of Homoleptic Sandwich Tris(pyrazolyl)borate Dysprosium (III) Cations via Intermolecular Dipolar Coupling

Journal:	*Dalton Transactions*
Manuscript ID	DT-ART-02-2019-000597.R2
Article Type:	Paper
Date Submitted by the Author:	09-May-2019
Complete List of Authors:	Alexandropoulos, Dimitris; Texas A&M University System, Chemistry Vignesh, Kuduva; Texas A&M University, Chemistry Xie, Haomiao; Texas A&M University System, Chemistry Dunbar, Kim; Texas A and M University, Chemistry

Journal Name

ARTICLE

Switching On Single-Molecule Magnet Properties of Homoleptic Sandwich Tris(pyrazolyl)borate Dysprosium (III) Cations via Intermolecular Dipolar Coupling

Received 00th January 20xx,
Accepted 00th January 20xx

DOI: 10.1039/x0xx00000x

www.rsc.org/

Dimitris I. Alexandropoulos,[a] Kuduva R. Vignesh,[a] Haomiao Xie,[a] and Kim R. Dunbar*[a]

Two new homoleptic Dy^{III} compounds $[Dy(Tp^{Me2})_2][DyCl_3(Tp^{Me2})]\cdot CH_2Cl_2$ (**1**) and $[Dy(Tp^{Me2})_2]I$ (**3**) as well as a heteroleptic $(NMe_4)[DyCl_3(Tp^{Me2})]$ (**2**) (Tp^{Me2} = tris(3,5-dimethylpyrazolyl)borate) species are reported. Magnetic studies revealed that **1** is a single-molecule magnet (SMM) with an energy barrier of U_{eff} = 80.7 K with $\tau_0 = 6.2 \times 10^{-7}$ s under a zero applied field. Compound **3** exhibits a U_{eff} of 13.5 K with $\tau_0 = 1.6 \times 10^{-6}$ s under a 0.08 T applied field. *Ab initio* CASSCF+RASSI-SO calculations were performed to further investigate the magnetic behavior of complexes **1-3**. The results support experimental magnetic data for **1** and **3** and indicate that an intermolecular dipolar interaction of (zJ = -0.1 cm^{-1}) is responsible for the SMM behavior of **1**.

Introduction

Single molecule magnets (SMMs), molecules that exhibit slow relaxation of their magnetization and magnetic hysteresis at a molecular level,[1] have captured the attention of the scientific community due to their fundamental quantum properties as well as their potential for applications in magnetic data storage[2] and quantum computing.[3] The performance of an SMM is affected by two critical parameters, *viz*., the magnetic anisotropy and the electronic structure of individual metal complexes that exhibit a well-isolated bistable ground state.[4] A natural target for this research is the chemistry of lanthanide ions, especially Dy^{III} and Tb^{III}, which possess remarkably large single-ion anisotropies. Compounds of these rare earth metal ions have accounted for most of the recent forefront developments in the field of SMMs as evidenced by very high energy barriers to the magnetization reversal (U_{eff}) and magnetic blocking temperatures (T_B).[5]

Nowadays, much effort has been directed at the synthesis of mononuclear Ln SMMs rather than polynuclear compounds.[6] The hypothesis of this idea is to harness the maximum magnetic anisotropy from a lanthanide ion by choosing ligands that affect, in a critical manner, the strength and the symmetry of the crystal field in highly symmetric or low-coordinate systems.[7, 8] This strategy has produced several families of compounds including sandwich-type complexes that exhibit extraordinary SMM properties. The first Ln-SMM of this type was reported[9] in 2003, a sandwich complex that features a terbium(III) ion and two phthalocyanine ligands with U_{eff} values as high as 938 K.[10] In 2011, slow magnetic relaxation was observed in the organometallic [(Cp^*)Er(COT)] (Cp* = pentamethylcyclopentadienide, COT = cyclooctatetraenide) complex.[11] After this discovery, several organolanthanide "sandwich-type" complexes were reported with cyclopentadienyl (Cp)[12] or cyclooctatetraenyl-based (COT)[13] ligands. Remarkably, the highly sterically congested compounds $[(Cp^{ttt})_2Dy][B(C_6F_5)_4]$ (Cp^{ttt} = 1,2,4-tri(tert butyl)cyclopentadienide)[14] and [(Cp*)Dy(Cp^{iPr5})][$B(C_6F_5)_4$] (Cp^{iPr5} = penta-iso-propylcyclopentadienyl)[15] exhibit magnetic hysteresis up to 60 and 80 K, respectively.

Recently we turned our attention to the synthesis of homoleptic lanthanide sandwich-type complexes using non-organometallic ligands in order to understand how their structural and electronic properties would affect the overall magnetic behavior. In this vein, tris(pyrazolyl)borates (Tp) provide an alternative to the most widely used cyclopentadienyl (Cp) derivatives.[16] Both ligand systems are monoanionic and, although Tp ligands are not as electronically tunable as Cp, they offer a wide range of steric profiles owing to the ease of substitution in the 3- and 5-positions of the pyrazolyl rings.[16] Thus, by choosing the appropriate substituents, coordination of solvents or anions can be avoided resulting in lower coordination environments than are typically found for lanthanide ions. The Tp ligand chemistry has been successfully employed for the synthesis of homoleptic divalent lanthanide complexes[17, 18, 19] or heteroleptic trivalent species.[20] Homoleptic

[a] Department of Chemistry, Texas A&M University, College Station, Texas 77843, USA. Email: dunbar@chem.tamu.edu

† † Electronic Supplementary Information (ESI) available: Crystal data and refinement parameters, reduced magnetization data, ac susceptibility measurements, and details of the theoretical analysis for complexes **1-3**. CCDC 1877238-1877240. For ESI and crystallographic data in CIF or other electronic format see DOI: 10.1039/x0xx00000x

Ln^{III} sandwich-type complexes are very rare,[17, 18] however and their magnetic properties are still unexplored.

Herein, we report the high-yield syntheses, structures, and magnetic properties of three new mononuclear low-coordinate complexes $[Dy(Tp^{Me2})_2][DyCl_3(Tp^{Me2})]$ (**1**), $(NMe_4)[DyCl_3(Tp^{Me2})]$ (**2**), and $[Dy(Tp^{Me2})_2]I$ (**3**) with the nitrogen donor ligand tris(3,5-dimethylpyrazolyl)borate (Tp^{Me2}). In these compounds, the Dy^{III} ions are six-coordinate adopting an elongated trigonal antiprismatic (trigonally distorted octahedral) geometry. Complexes **1** and **3** constitute rare examples of sandwich-type complexes in which lanthanide ions are in a LnN_6 coordination environment.[21]

Experimental Section

Syntheses

All manipulations were carried out under an inert atmosphere of N_2 using standard Schlenk and glovebox techniques unless otherwise noted. The starting material KTp^{Me2} was prepared using literature procedures,[22] dried under vacuum at 100° C and stored in the glovebox prior to use. Anhydrous $DyCl_3$ and THF without butylated hydroxytoluene as an inhibitor were purchased from Sigma Aldrich and stored under an inert atmosphere. CH_2Cl_2 was purchased from Sigma Aldrich, dried over molecular sieves, distilled and stored over fresh molecular sieves in an inert atmosphere prior to use.

$[Dy(Tp^{Me2})_2][DyCl_3(Tp^{Me2})]\cdot CH_2Cl_2$ (1). To a colorless solution of KTp^{Me2} (0.34 g, 1.0 mmol) in THF (30 mL) was added solid $DyCl_3$ (0.13 g, 0.5 mmol) and the solution was stirred overnight. The solvent was removed under vacuum, and the crude material was extracted using 10 mL of CH_2Cl_2 which was filtered and layered with Et_2O (10 mL). Slow diffusion after 1 day yielded colorless blocks of **1** which were collected by filtration and washed with Et_2O (3 x 5 mL); yield 65% (0.43 g). Anal. Calc. for $C_{45}H_{66}N_{18}B_3Cl_3Dy_2$ **(1)**: C, 40.86; H, 5.03; N, 19.06 %. Found: C, 40.75; H, 5.07; N, 18.98 %. Selected ATR data (Nujol mull, cm^{-1}): 1541 (s), 1265 (w), 1202 (s), 1136 (s), 1085 (m), 1043 (s), 1021 (m), 980 (w), 929 (w), 840 (w), 808 (m), 781 (m), 739 (m), 702 (m), 650 (m), 611 (w), 567 (w), 457 (w).

$(NMe_4)[DyCl_3(Tp^{Me2})]$ (2). To a colorless solution of KTp^{Me2} (0.34 g, 1.0 mmol) in THF (30 mL) was added solid $DyCl_3$ (0.13 g, 0.5 mmol) and NMe_4Cl (0.22 g, 2.0 mmol). After the reaction was stirred overnight the solvent was removed under vacuum, and the crude material was extracted with 10 mL of CH_2Cl_2. The extract was filtered and the solution was layered with Et_2O (10 mL) to yield colorless plates of **2** after 24 h whiach were collected by filtration and washed with Et_2O (3 x 5 mL); yield 50% (0.32 g). Anal. Calc. for $C_{19}H_{34}N_7BCl_3Dy$ **(2)**: C, 35.65; H, 5.35; N, 15.32 %. Found: C, 35.57; H, 5.39; N, 15.28 %. Selected ATR data (Nujol mull, cm^{-1}): 1539 (m), 1199 (m), 1069 (m), 1042 (m), 944 (m), 842 (m), 806 (w), 722 (m), 698 (m), 645 (m), 457 (w).

$[Dy(Tp^{Me2})_2]I$ (3). To a colorless solution of KTp^{Me2} (0.34 g, 1.0 mmol) in THF (30 mL) was added solid $DyCl_3$ (0.13 g, 0.5 mmol) and NaI (0.30 g, 2.0 mmol). After stirring for 12 h, the solvent was removed under vacuum, and the crude material was extracted using 10 mL of CH_2Cl_2, filtered and layered with Et_2O (10 mL). Slow mixing gave after 1 day led to colorless blocks of **1** which were collected by filtration and washed with Et_2O (3 x 5 mL); yield 60% (0.27 g). Anal. Calc. for $C_{30}H_{44}N_{12}B_2IDy$ **(1)**: C, 40.77; H, 5.02; N, 19.02 %. Found: C, 40.71; H, 4.98; N, 19.05 %. Selected ATR data (Nujol mull, cm^{-1}): 1534 (s), 1413 (s), 1354 (s), 1186 (s), 1147 (m), 1125 (w), 1071 (s), 1043 (s), 987 (m), 827 (m), 803 (m), 722 (w), 698 (m), 646 (m), 458 (m).

Single crystal X-ray crystallography

Crystals of **1**·CH_2Cl_2, **2** and **3** were immersed in ®Paratone oil and selected under ambient conditions using a MiTeGen microloop. The crystals were placed in a stream of cold N_2 at 110(1) K on a Bruker D8-QUEST diffractometer equipped with a IμS Mo microsource (λ = 0.71073 Å). An initial unit cell was determined using SAINT[23] from a set of 3 ω-scans consisting of 30 0.5° frames and a sweep width of 15°. From this unit cell, a data collection strategy was used to collect all independent reflections to a resolution of at least 0.82 Å using APEX3.[23] Full details of the data collections are presented in Table S1. The Cambridge Crystallographic Database Centre numbers for each complex are: 1877238 for **1**, 1877239 for **2**, and 1877240 for **3**. The data were corrected for absorption using SADABS-2014/5.[24] The space groups were determined from analysis of the systematic absences and E-statistics using XPREP. The structures were solved using the intrinsic phasing routine in SHELXT.[25] Non-hydrogen atoms were located from the Fourier difference map and refined using a least-squares refinement algorithm in SHELXL-2014[26] within the OLEX[27] program. All non-hydrogen atoms were refined anisotropically and hydrogen atoms were placed in calculated positions and refined with thermal parameters constrained to their parent atom. Specific details of the structure refinements are presented below. The programs used for molecular graphics were DIAMOND[28] and MERCURY.[29]

Ab initio calculations

Using MOLCAS 8.0,[30] *ab initio* calculations with CASSCF/RASSI-SO/SINGLE_ANISO methods were performed on the Dy^{III} ions using the crystal structures of **1-3** to rationalize the observed SMM behavior. The neighboring Dy^{III} center was substituted with a Lu^{III} ion in **1** while computing the single-ion anisotropy of the other Dy center. Relativistic effects were taken into account on the basis of the Douglas−Kroll Hamiltonian.[31] The spin-free eigenstates were achieved by the Complete Active Space Self-Consistent Field (CASSCF) method.[32] The basis sets were taken from the ANORCC library for the calculations.[33] We employed the [ANO-RCC... 8s7p5d3f2g1h.] basis set for Dy^{III} atoms, the [ANO-RCC...5s4p2d.] basis set for Cl atoms, the [ANO-RCC...3s2p.] basis set for C atoms, the [ANO-RCC...2s.] basis set for H atoms, the [ANO-RCC...4s3p2d1f.] basis set for N atoms, the [ANO-RCC...7s6p4d2f.] basis set for the Lu atom, and the [ANO-RCC...3s2p1d.] basis set for B atoms. In the first step, we run a guessorb calculation using a Seward module to create the starting guess orbitals. We included nine electrons across seven 4f orbitals of the Dy^{III} ion. Then using these guess orbitals, we chose the active space based on the number of active electrons

in the number of active orbitals and carried out the SA-CASSCF calculations. The Configuration Interaction (CI) procedure was computed for the Dy^{III} ion which considered twenty-one sextet excited states in the calculations to compute the anisotropy. After computing these excited states, we used the RASSI-SO[34] module to calculate the spin-orbit (SO) coupled states. Moreover, these computed SO states were considered in the SINGLE_ANISO[35] program to compute the *g*-tensors. The *g*-tensors for the Kramers doublets (KDs) of Dy^{III} were computed based on the pseudospin S = ½ formalism.[35] Crystal-Field (CF) parameters were extracted using the SINGLE_ANISO code, as implemented in MOLCAS 8.0. The CF parameters were analyzed for deeper insight into the mechanism of magnetic relaxation. The corresponding crystal field Hamiltonian is given in equation 1:

$$\widehat{H}_{CF} = \sum\sum_{k=-q}^{q} B_k^q \widetilde{O}_k^q \qquad (1)$$

Where B_k^q is the crystal field parameter, and O_k^q is the Steven's operator.

The intermolecular dipolar interactions between the two Dy^{III} ions in the crystal structure of **1** were computed by fitting the experimental magnetic data using the POLY_ANISO program.[36]

Results and Discussion

Syntheses

Compound **1** was prepared by the reaction of $DyCl_3$ with 2 equivalents of KTp^{Me2} in THF. The solvent was removed under vacuum and the residue was recrystallized from CH_2Cl_2/Et_2O. Addition of an excess of solid NMe_4Cl in the reaction mixture of **1** led to the formation of **2**, while the addition of excess NaI led to the isolation of compound **3**. The chemical and structural identities of the compounds were confirmed by single-crystal X-ray crystallography, elemental analyses (C, H,

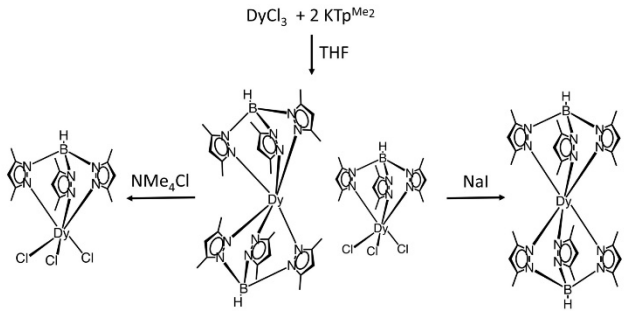

Scheme 1. Synthesis of **1-3**.

Structural Determination

Compound **1** crystallizes in the monoclinic space group $P2_1/n$. The asymmetric unit features one $[Dy(Tp^{Me2})_2]^+$ cation, one $[DyCl_3(Tp^{Me2})]^-$ anion and one CH_2Cl_2 solvent molecule. The Dy^{III} ions are 6-coordinate in both ions in**1** (Fig. 1). The $[Dy(Tp^{Me2})_2]^+$ cation adopts a bent sandwich-type structure with a B-Dy-B angle of 169.57(3)°. The Dy^{III} ion is surrounded only by nitrogen donor atoms with all coordination sites being occupied by two chelating Tp^{Me2} ligands, which are staggered with respect to each other. In contrast, the coordination sphere of the Dy^{III} anion consists of three nitrogen atoms from one tridentate Tp^{Me2} ligand with the remaining positions being filled by three terminal chloride ions. Compound **2** contains the discrete $[DyCl_3(Tp^{Me2})]^-$ moiety, which is isostructural to that of **1** but is

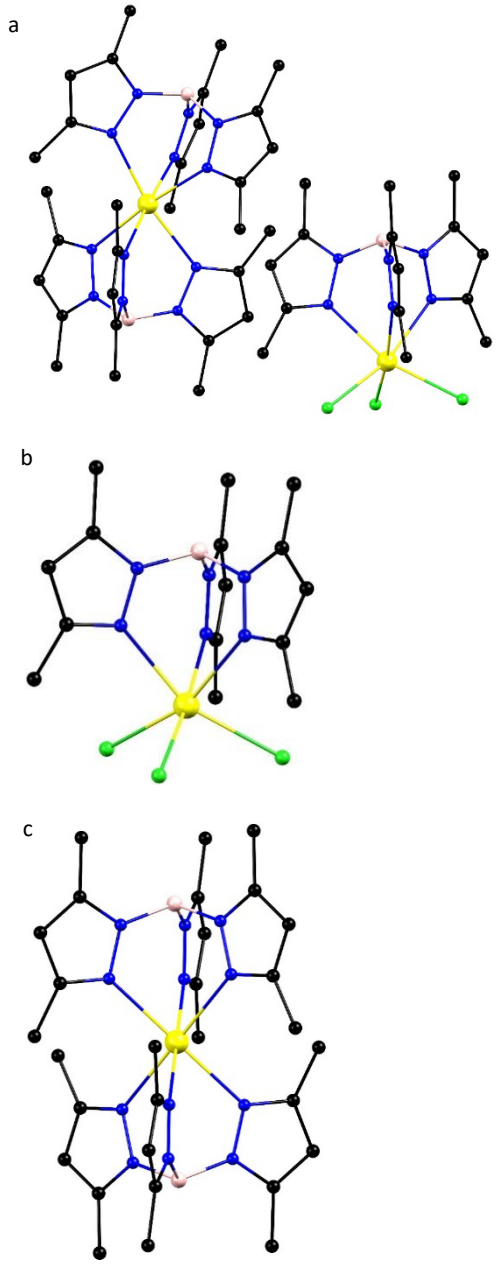

Fig. 1 Crystal structures of compound **1** (a), anion **2** (b), and cation **3** (c). Colors: Dy, yellow; N, blue; B, pink; Cl, green, C, black. H atoms are omitted for the sake of clarity.

co-crystallized with one NMe_4^+ cation in the $P2_1/n$ space group. The structure is similar to the recently reported neutral

[$DyCl_3$(Tpm)] complex,[37] containing the isoelectronic tris(pyrazolyl)methane (Tpm) ligand. Compound **3** is isomorphous to the previously reported Sm^{III} analogue,[18] consisting of well-separated $[Dy(Tp^{Me2})_2]^+$ cations and iodide anions. The cation in **3** lies on a 2/*m* symmetry element, with a mirror plane passing through two of the pyrazolyl rings. The crystal packing of **1-3** (SI) reveals well-isolated cationic and ionic moieties. The closest intermolecular Dy···Dy contacts are 7.969(2) Å (between two cations) and 9.145(2) Å (between cations and anions) for **1**, 8.895(5) Å and, 8.399(5) Å, for **2** and **3**, respectively.

In order to evaluate the symmetry of the inner coordination spheres of the dysprosium ions in **1-3**, specific key structural parameters were evaluated and SHAPE measures[38] were performed (Table S3). In both cations **1** and **3**, Dy^{III} ions are coordinated to two tripodal Tp^{Me2} ligands. In the discrete cation **1**, the Dy-N bond distances are nearly equal, ranging from 2.366(2) to 2.383(2). The intra-ligand bite angles (N_{TpMe2}-Dy-N_{TpMe2}) are acute (77.39(8)-83.68(8)°), with the inter-ligand *cis* N_{TpMe2}-Dy-$N_{TpMe2'}$ angles being obtuse (91.59(8)-106.38(7)°) (Table S2). These parameters suggest a trigonal elongation which is further evidenced by the fact that the N-N distances within the planes defined by the nitrogen donor atoms of each Tp^{Me2} ligand (planes N1-N3-N5 and N7-N9-N11, 2.964(3)-3.169(3) Å) are significantly shorter than those between the two planes (N1-N7/N9, N3-N7/N11, N5-N9/N11; 3.405(3)-3.801(3) Å). Also, the distance (d_b) between the two planes is 3.148(3), much longer than the distances (d_s) between three pairs of side planes, 2.568(3)-2.597(3) Å, giving $\delta = d_b - d_s$ as 0.565 Å ($\delta = 0$ for ideal octahedral geometry).[39] These metrical parameters indicate that the Dy^{III} ion in cation **1** adopts a distorted coordination geometry which is best described as elongated trigonal antiprismatic. This geometry has been previously observed for divalent lanthanide[17, 18, 19] and transition metal complexes with two claw-type tridentate ligands.[40]

Fig. 2 Labelled representation of the cation in **1** (left) and in **3** (right), emphasizing the coordination geometry of the Dy atom. Colors: Dy, yellow; N, blue; B, pink; Cl, green, C, black. H atoms are omitted for the sake of clarity.

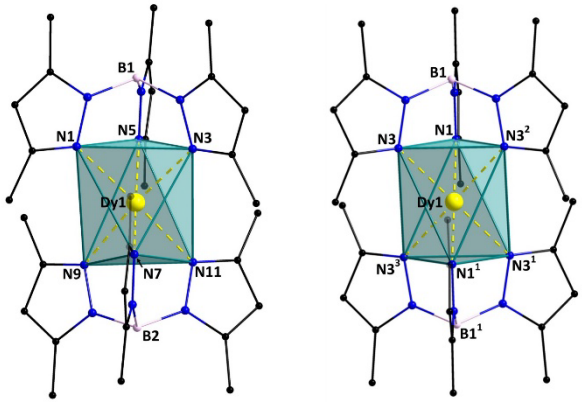

Interestingly, the Dy atom in cation **3** adopts a similar geometry to **1** with some notable differences. Firstly, the two independent Dy-N bond distances, 2.376(2) and 2.430(3) Å, are larger compared to those of **1**. Moreover, due to the crystallographic symmetry, the two planes defined by the nitrogen donor atoms of each Tp^{Me2} ligand are parallel, whereas in **1** the angle between the planes is 10.53(2)°. In addition, both the Tp^{Me2}-Dy-Tp^{Me2} and B-Dy-B angles in **3** (178.64(2)° and 180.00(2)°), are larger than those of **1** (173.05(2)° and 169.57(2)°), indicating that cation **3** exhibits a more compact and linear structure than the cation in **1**. Finally, the discrete $[DyCl_3(Tp^{Me2})]^-$ anion is in a very similar trigonal antiprismatic coordination geometry with bond distances and angles being in the same ranges as **1** and **2**.

DC Magnetic Measurements

The static direct current (*dc*) magnetic properties of **1-3** were measured from 2 to 300 K in a 0.1 T applied field (Fig. 3). The experimental $\chi_M T$ value at 300 K for **1** (28.23 cm^3 K mol^{-1}) is in good agreement with the theoretical value (28.34 cm^3 K mol^{-1}) expected for two non-interacting Dy^{III} ($^6H_{15/2}$, $S = 5/2$, $L = 5$, $g = 4/3$) ions. The $\chi_M T$ values at 300 K for **2** and **3** (14.12 cm^3 K mol^{-1} and 14.15 cm^3 K mol^{-1}, respectively) are in accord with the calculated value for a single Dy^{III} ion (14.17 cm^3 K mol^{-1}).[41] Compounds **1-3** exhibit similar behavior, with $\chi_M T$ decreasing slightly from 300 K to reach a value at 100 K of 27.04 cm^3 K mol^{-1} for **1**, 13.78 cm^3 K mol^{-1} for **2**, and 13.64 cm^3 K mol^{-1} for **3**. Below this temperature, $\chi_M T$ decreases more rapidly to a minimum value at 2.0 K of 23.48 cm^3 K mol^{-1} for **1**, 8.06 cm^3 K mol^{-1} for **2**, and 10.80 cm^3 K mol^{-1} for **3**. This behavior below 100 K is attributed to magnetic anisotropy and/or depopulation of the excited Stark sublevels of the Dy^{III} ions.

Fig. 3 Temperature dependence of $\chi_M T$ for **1-3**. Solid lines are the *ab initio* calculated data.

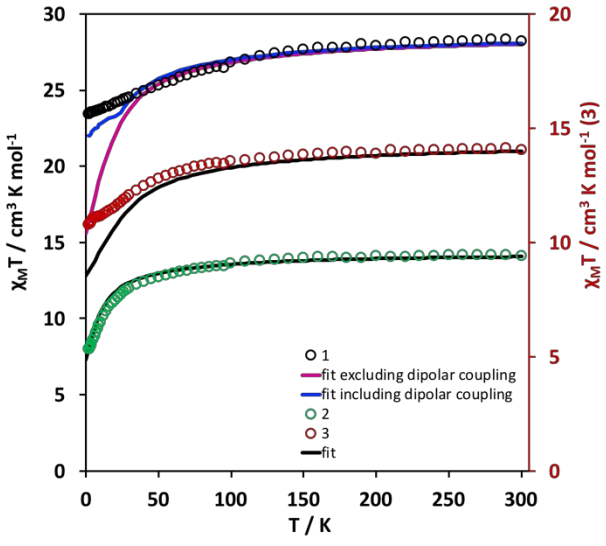

Field-dependent magnetization measurements were performed on **1-3** at different low temperatures and magnetic fields (Fig. 4). The M versus H plots for **1-3** at 2 K show a rapid increase below 1 T followed by a slow, nearly linear increase up to 11.51 μ_B, 6.44 μ_B and 6.18 μ_B, for **1**, **2** and **3**, respectively. The

lack of saturation in magnetization as well as the fact that the values at 7 T are lower that the theoretical ones (21.28 μ_B for **1** and 10.64 for **2** and **3** μ_B)[41] indicates the presence of magnetic anisotropy and/or population of low-lying excited states. This conclusion is further supported by the reduced magnetization data (SI) where the isofield lines do not superimpose on a single master curve but slightly deviate from one another, indicating non-negligible magnetic anisotropy.

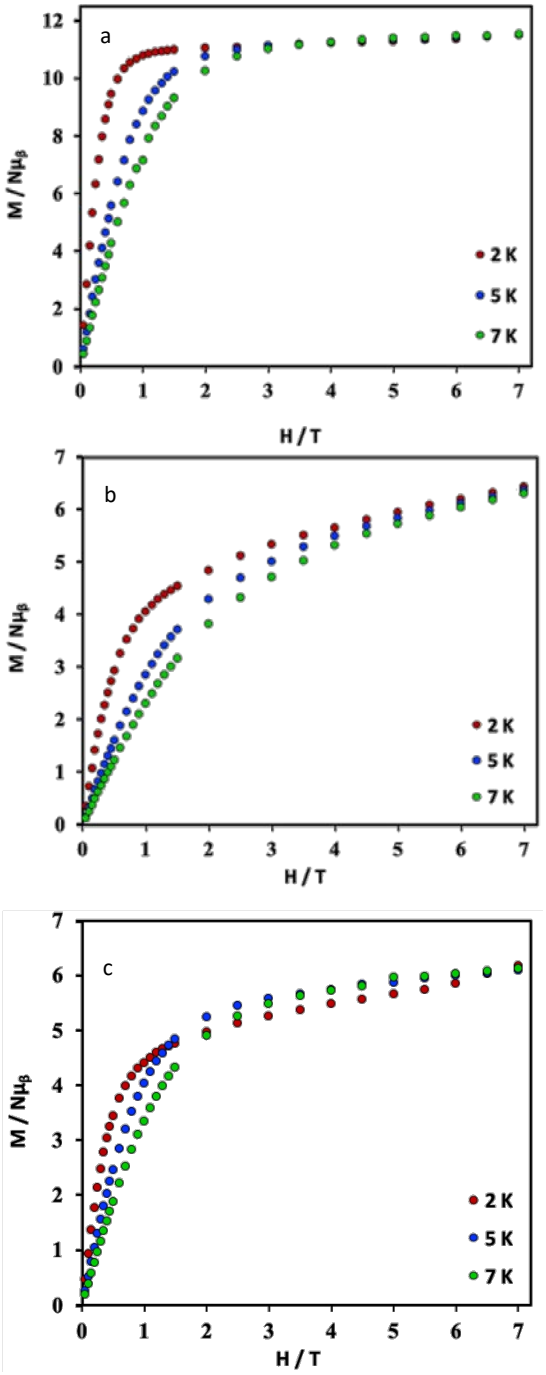

Fig. 4 M vs. H plots for **1** (a), **2** (b), and **3** (c) at different low temperatures and magnetic fields.

AC Magnetic Measurements

The dynamic magnetic properties of **1**-**3** were probed by alternating current (*ac*) magnetic susceptibility studies performed from 2-18 K using a 2 Oe ac field oscillating at frequencies in the 1-1000 Hz range. Compound **1** exhibits frequency-dependent out-of-phase χ_M'' signals in a zero applied dc field, with well-resolved peak maximum appearing below ~12 K that shift to lower frequency as the temperature decreases, indicating the presence of slow magnetic relaxation. Given that **1** contains two different paramagnetic ionic units, one may hypothesize that the SMM properties could originate from the single-ion anisotropy effects of either the $[Dy(Tp^{Me2})_2]^+$ or $[DyCl_3(Tp^{Me2})]^-$ ions or the intermolecular interactions between them. This being the case, in order to determine the

Fig. 5 Out-of-phase (χ'') component of the magnetic susceptibility vs.

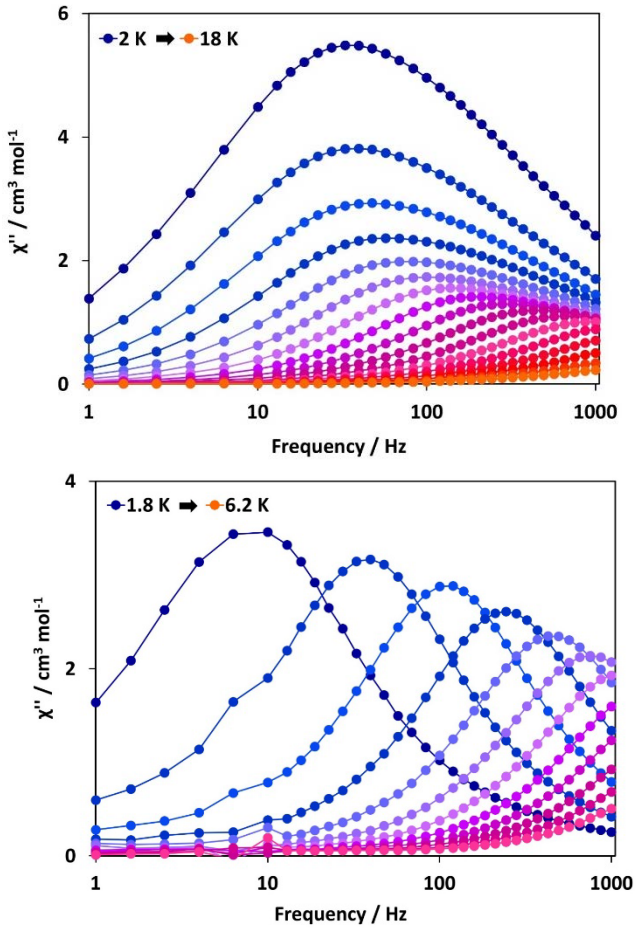

frequency for **1** (top) and **3** (bottom).

origin of the SMM behavior of **1**, measurements of the *ac*

magnetic susceptibility as a function of temperature also were performed on **2** and **3** which contain only the $[DyCl_3(Tp^{Me2})]^-$ anion and the $[Dy(Tp^{Me2})_2]^+$ cation, respectively. In fact, these studies did not reveal any slow relaxation for **2** in dc fields from 0-0.2 T (SI) and for **3**, no out-of-phase *ac* susceptibility signals were observed in a zero dc field, an indication of the presence of significant quantum tunneling of the magnetization (QTM). Application of an optimal 0.08 T dc field was sufficient to quench QTM and to observe dominant Orbach relaxation (SI). The absence of SMM behavior in **2** and **3**, under a zero dc field clearly supports the conclusion that the slow magnetic relaxation observed for **1** is a consequence of minor changes in the coordination geometry of the Dy^{III} ion, and/or intermolecular dipolar interactions between the anionic and cationic moieties.

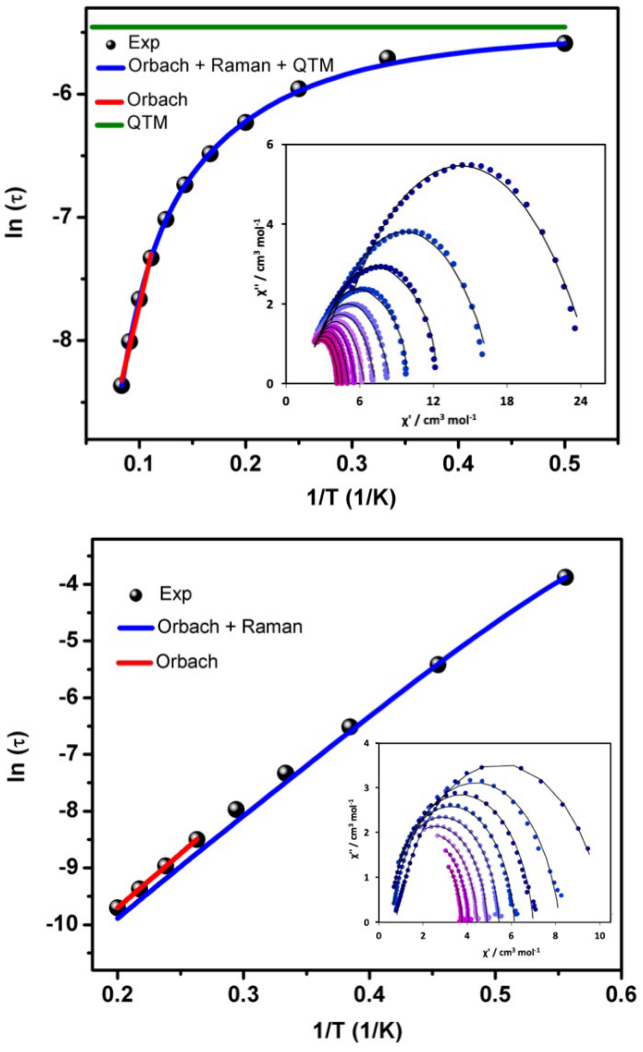

Figure 6. Temperature dependence of the magnetic relaxation rate ln(τ) for **1** (top) and **3** (bottom). Solid black points are the relaxation rates extracted from the CC-fit. Solid color lines are fits as labeled. Inset: Cole-Cole plot for **1** and **3** obtained using the ac susceptibility data in a zero and 0.08 T applied *dc* field, respectively. The solid lines correspond to the best fit obtained with a generalized Debye model.

The experimental data for **1** and **3** were fit using a generalized Debye model in CC-fit[42] to extract τ and α parameters, considering a single relaxation process (Fig. S16). The relaxation times for both **1** and **3** were plotted as ln(τ) vs. 1/T in Fig. 6 and the data were analyzed by the following equation[21]:

$$\tau^{-1} = \tau_{QTM}^{-1} + CT^n + \tau_0^{-1}\exp\left(-\frac{U_{eff}}{k_B T}\right) \quad (2)$$

where τ_{QTM}^{-1}, CT^n, and $\tau_0^{-1}\exp(-U_{eff}/k_BT)$ represent QTM, Raman, and Orbach relaxation processes, respectively. The fitting yielded: U_{eff}/k_B = 80.7 K, $\tau_0 = 6.2 \times 10^{-7}$ s, n = 5.7 and C = 0.24 s^{-1} $K^{-5.7}$ for **1** and U_{eff}/k_B = 13.5 K, $\tau_0 = 1.6 \times 10^{-6}$ s, n = 6 and C = 0.1 s^{-1} K^{-6} for **3**. The n value is lower than the expected value for a Kramers ion which is ascribed to the presence of both optical and acoustic Raman processes involving magnetic relaxation.[43] A τ_{QTM}^{-1} of 0.004 s was obtained for **1**, while we consider $\tau_{QTM}^{-1} = 0$ for **3**.

Ab initio calculations

Ab initio calculations were carried out to identify the mechanism(s) of magnetic relaxation for **1**–**3** using CASSCF/RASSI-SO/SINGLE_ANISO methods (see computational details). This methodology has been widely used to precisely rationalize the mechanism of magnetic relaxation of Dy^{III} ions.[7, 44, 45] The cationic $[Dy(Tp^{Me2})_2]^+$ unit is referred to as Dy1 and the anionic $[DyCl_3(Tp^{Me2})]^-$ unit is referred to as Dy2 for **1**. The ground state g-tensors of Dy^{III} ions in **1-3** are listed in Table 1. The calculated g_z values for all the Dy^{III} ions do not approach the value of ~20 expected for a pure Ising $|m_J = \pm 15/2>$ multiplet and the transverse components (g_x and g_y) are large. These findings indicate a strong mixing of the wavefunctions that would enhance the presence of quantum tunneling of magnetization (QTM) in ground KDs.

Table 1. *Ab initio* Computed Energies of the Lowest Kramers Doublets (KDs) and Ground-State *g*-Tensors of Dy^{III} ions in **1-3**.

KDs	Complex 1		Complex 2	Complex 3
	Dy1	Dy2		
1	0.0	0.0	0.0	0.0
2	53.3	24.4	18.6	59.5
3	59.0	56.0	48.8	79.4
4	174.9	121.7	119.8	166.1
5	301.1	226.5	224.7	287.9
6	390.5	271.9	244.5	354.2
7	526.1	284.1	283.1	495.3
8	614.4	348.1	404.3	583.8
g_x	0.3864	0.3617	0.6488	0.4198
g_y	1.0861	2.9738	2.2813	0.9999
g_z	16.4112	14.7872	15.1077	16.4851

Fig. 7 *Ab initio* computed magnetization reversal barrier for Dy1 (a) and Dy2 (b) for **1**, **2** (c) and **3** (d). The thick blue line indicates the Kramers doublets (KDs) as a function of computed magnetic moment. The double red arrows represent the presence of QTM/TA-QTM between the connecting pairs. The purple/green arrows show the possible pathway via Orbach/Raman relaxation. The numbers

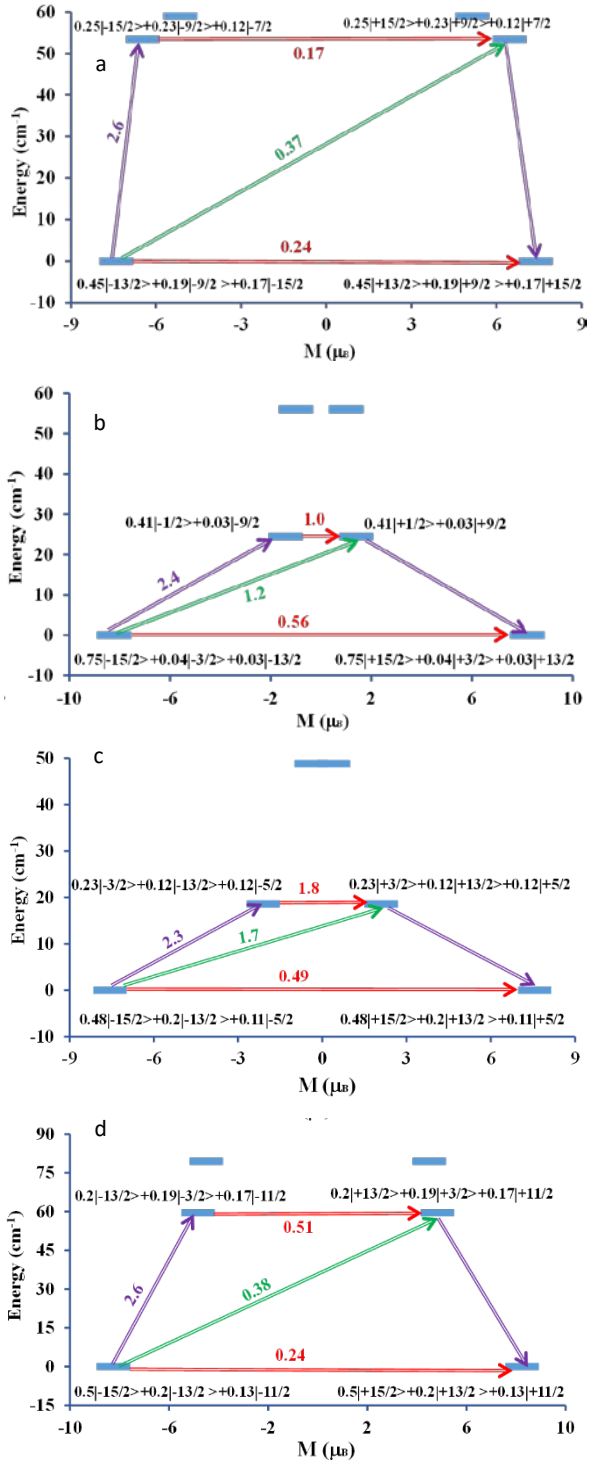

provided at each arrow are the mean absolute value for the corresponding matrix element of transition magnetic moment.

The computed energies of the eight low-lying Kramers doublets are provided in Table 1 and Table S6. The eight KDs span energy ranges of 614.4 cm^{-1} and 348.1 cm^{-1} for Dy1 and Dy2 ions in **1**, and 404.3 cm^{-1} and 583.8 cm^{-1} for **2** and **3**, respectively. We constructed relaxation mechanisms for magnetization blockade for each complex (Figure 7) to compute the energy barriers. Calculations yielded a ground-to-first excited state KD energy gap of 53.3 cm^{-1} (76.7 K) for Dy1 and 24.4 cm^{-1} (35.1 K) for Dy2 in **1**, and 18.6 (26.8 K) cm^{-1} for **2** and 59.5 cm^{-1} (85.6 K) for **3**. The ground state KDs of the Dy^{III} ions in **1**–**3** have sufficient QTM contributions, thus allowing for the magnetization to relax via ground states and predicts the absence of SMM behavior in zero field. The QTM probability of ground state KDs can be described by the Crystal-Field (CF, B_k^q) parameters. The computed CF parameters for **1-3** are provided in Table S6 in SI.

The QTM process is dominant when the non-axial terms (for which $q \neq 0$ and $k = 2, 4, 6$) are larger as compared to the axial ones (for which $q = 0$ and $k = 2, 4, 6$).[45, 46] For all the Dy^{III} ions in **1**-**3**, there is significant transverse anisotropy and fast QTM relaxation.[47] The cationic Dy1 units in **1** and **3**, however, have relatively small TA-QTM (Temperature Assisted-QTM) in the first excited states. This situation can assist in magnetization relaxation via the first excited states when a dc field is applied.

Another possibility to achieve SMM behavior at zero dc field is the presence of intermolecular dipolar interactions with another paramagnetic moiety. Interestingly the latter case is possible for **1** due to the presence of the anionic Dy2 site. In **3**, there are no other paramagnetic metal centers and SMM behavior is observed by applying a field of 0.08 T. The experimentally extracted energy barrier of 15.7 K is small compared to the computed one (85.6 K) which may be correlated to the exclusion of intermolecular interactions and other possible pathways such as spin-phonon relaxation.[45, 48]

Given that single-ion calculations do not agree with the observed SMM behavior of **1**, we further developed an exchange coupled states relaxation mechanism considering only the intermolecular dipolar coupling (z*J*) between Dy^{III} ions in **1** using the POLY_ANISO program[36] within the Lines model.[49]

Table 2. Lowest exchange coupled doublets (cm^{-1}) arising from the intermolecular dipolar coupling, the corresponding tunnel splitting (Δ_{tun}, cm^{-1}), and the g_z value of each doublet (g_x and $g_y \neq 0$) for complex **1**.

No.	E(cm^{-1})	Δ_{tun}	g_z
1	0.000000000000 0.000825740851	8.3×10^{-4}	27.505016758
2	0.030008594656 0.030123597408	1.2×10^{-4}	13.629521004
3	24.433242399548 24.433470832143	2.3×10^{-4}	24.939571354
4	24.488581708821 24.488797960412	2.2×10^{-4}	13.276317692
5	53.342120474274 53.342729320503	6.1×10^{-4}	12.580147724
6	53.378652032718 53.379458668274	8.1×10^{-4}	30.292134051
7	56.015025473425 56.015520080294	5.0×10^{-4}	13.727491670
8	56.084943106477 56.085596191977	6.5×10^{-4}	25.539879794
9	59.020608284673 59.021867645331	1.3×10^{-3}	14.543046827
10	59.029733983718 59.030350402723	6.2×10^{-4}	23.041728525
11	77.790507697369 77.792706339706	2.2×10^{-3}	17.768208806
12	77.818807178604 77.821119986496	2.3×10^{-3}	21.649981202

The magnetic susceptibility data for **1** are well reproduced (see Figure 3) with the inclusion of a relatively large intermolecular dipolar interaction (z*J* = -0.1 cm^{-1}) which is in agreement with the calculated energy barrier. It is obvious that dipolar interactions help to reduce the tunneling gap (Δ_{tun}) between the ground exchange coupled state (Table 2) and to fewer higher excited states as well. The tunneling gap becomes large (~10^{-3}) at eighth excited states,[45,50] which leads the magnetic relaxation in these states with an energy barrier of 59 cm^{-1} (85 K). This supports the observation of maxima in the experimental out-of-phase ac magnetic susceptibilities under zero dc field. This calculated energy barrier is in good agreement with the experimentally extracted energy barrier of 80.7 K. The discrepancy between the observed and the calculated magnetization values can be rationalized with the non-inclusion of other factors such as hyperfine interactions and spin-phonon interactions in the calculation (Fig. S13-S15).

Conclusions

In this work, we described the synthesis and detailed magnetic analysis of two new compounds with the sandwich-type $[Dy(Tp^{Me2})_2]^+$ moiety. In this cation the Dy^{III} ion is six-coordinate with a trigonally elongated octahedral geometry in both compounds **1** and **3**. Interestingly, slow relaxation of the magnetization was observed only for **1**, whereas in **3** QTM dominates below 20 K. Fitting of the data, considering all possible relaxation pathways, gave an energy barrier U_{eff} = 80.7 K with $\tau_0 = 6.2 \times 10^{-7}$ s for **1**, under a zero applied field, and U_{eff} = 13.5 K with $\tau_0 = 1.6 \times 10^{-6}$ s for **3**, under a 0.08 T applied field. In order to explain the magnetic behavior of **1** versus that of **3**, *ab initio* calculations were performed which revealed that the presence of strong intermolecular dipolar interactions are responsible for the SMM behavior of complex **1**. These findings demonstrate that such interactions can have a large impact on the SMM properties of simple lanthanide complexes. In order to further explore the magnetic properties of Tp compounds, this chemistry will be extended to other anisotropic 4f metal ions as well as to different tris(pyrazolyl)borate (Tp) derivatives. In the latter case, we will study how deviations of the B-Ln-B angle from linearity, imposed by the steric properties of the ligand, affect the magnetic behavior of the compounds.

Conflicts of interest

There are no conflicts to declare.

Acknowledgements

We gratefully acknowledge support for this work by the National Science Foundation (CHE-1808779) and the Robert A. Welch Foundation (Grant A-1449). The SQUID magnetometer was purchased with funds provided by the Texas A&M University Vice President of Research. We are grateful to the HPRC at Texas A&M for the computing resources.

Notes and references

1. G. Christou, D. Gatteschi, D. N. Hendrickson and R. Sessoli, *MRS Bulletin*, 2000, **25**, 66-71; R. Bagai and G. Christou, *Chem. Soc. Rev.*, 2009, **38**, 1011-1026.
2. R. Sessoli, D. Gatteschi, A. Caneschi and M. A. Novak, *Nature*, 1993, **365**, 141.
3. E. Moreno-Pineda, C. Godfrin, F. Balestro, W. Wernsdorfer and M. Ruben, *Chem. Soc. Rev.*, 2018, **47**, 501-513.
4. J. D. Rinehart and J. R. Long, *Chem. Sci.*, 2011, **2**, 2078-2085.
5. D. N. Woodruff, R. E. P. Winpenny and R. A. Layfield, *Chem. Rev.*, 2013, **113**, 5110-5148.
6. J. Tang and P. Zhang, in *Lanthanide Single Molecule Magnets*, 2015, DOI: 10.1007/978-3-662-46999-6_2, ch. Chapter 2, pp. 41-90; J. M. Frost, K. L. M. Harriman and M. Murugesu, *Chem. Sci.*, 2016, **7**, 2470-2491.
7. L. Ungur and L. F. Chibotaru, *Phys. Chem. Chem. Phys.*, 2011, **13**, 20086-20090.
8. N. F. Chilton, D. Collison, E. J. L. McInnes, R. E. P. Winpenny and A. Soncini, *Nat. Commun.*, 2013, **4**, 2551.
9. N. Ishikawa, M. Sugita, T. Ishikawa, S.-y. Koshihara and Y. Kaizu, *J. Am. Chem. Soc.*, 2003, **125**, 8694-8695.
10. C. R. Ganivet, B. Ballesteros, G. de la Torre, J. M. Clemente-Juan, E. Coronado and T. Torres, *Chem. Eur. J.*, 2012, **19**, 1457-1465.
11. S.-D. Jiang, B.-W. Wang, H.-L. Sun, Z.-M. Wang and S. Gao, *J. Am. Chem. Soc.*, 2011, **133**, 4730-4733.
12. B. M. Day, F.-S. Guo and R. A. Layfield, *Acc. Chem. Res.*, 2018, **51**, 1880-1889.

13. K. L. M. Harriman and M. Murugesu, *Acc. Chem. Res.*, 2016, **49**, 1158-1167.
14. F.-S. Guo, B. M. Day, Y.-C. Chen, M.-L. Tong, A. Mansikkamäki and R. A. Layfield, *Angew. Chem. Int. Ed.*, 2017, **56**, 11445-11449; C. A. P. Goodwin, F. Ortu, D. Reta, N. F. Chilton and D. P. Mills, *Nature*, 2017, **548**, 439.
15. F.-S. Guo, B. M. Day, Y.-C. Chen, M.-L. Tong, A. Mansikkamäki and R. A. Layfield, *Science*, 2018, **362**, 1400.
16. S. Trofimenko, *Chem. Rev.*, 1993, **93**, 943-980.
17. S.-Y. Liu, G. H. Maunder, A. Sella, M. Stevenson and D. A. Tocher, *Inorg. Chem.*, 1996, **35**, 76-81.
18. A. C. Hillier, Zhang, G. H. Maunder, S. Y. Liu, T. A. Eberspacher, M. V. Metz, R. McDonald, Â. Domingos, N. Marques, V. W. Day, A. Sella and J. Takats, *Inorg. Chem.*, 2001, **40**, 5106-5116.
19. M. Kühling, C. Wickleder, M. J. Ferguson, C. G. Hrib, R. McDonald, M. Suta, L. Hilfert, J. Takats and F. T. Edelmann, *New J. Chem.*, 2015, **39**, 7617-7625.
20. A. Lannes and D. Luneau, *Inorg. Chem.*, 2015, **54**, 6736-6743; G.-F. Xu, Q.-L. Wang, P. Gamez, Y. Ma, R. Clérac, J. Tang, S.-P. Yan, P. Cheng and D.-Z. Liao, *Chem. Commun.*, 2010, **46**, 1506-1508.
21. K. R. Meihaus, S. G. Minasian, W. W. Lukens, S. A. Kozimor, D. K. Shuh, T. Tyliszczak and J. R. Long, *J. Am. Chem. Soc.*, 2014, **136**, 6056-6068.
22. S. Trofimenko, J. R. Long, T. Nappier and S. G. Shore, in *Inorganic Syntheses*, John Wiley & Sons, Inc., 1970, DOI: 10.1002/9780470132432.ch18, pp. 99-109.
23. Bruker-AXS, *Journal*, 2015.
24. G. M. Sheldrick, *SADABS*, 1996.
25. G. M. Sheldrick, *Acta Crystallogr. Sect. A, Found. and Adv.*, 2015, **71**, 3-8.
26. G. M. Sheldrick, *Acta crystallogr. Sect. C, Struc. Chem.*, 2015, **C71**, 3-8.
27. O. V. Dolomanov, L. J. Bourhis, R. J. Gildea, J. A. K. Howard and H. Puschmann, *J. Appl. Crystallogr.*, 2009, **42**, 339-341.
28. W. Pennington, *J. Appl. Crystallogr.*, 1999, **32**, 1028-1029.
29. C. F. Macrae, P. R. Edgington, P. McCabe, E. Pidcock, G. P. Shields, R. Taylor, M. Towler and J. van de Streek, *J. Appl. Crystallogr.*, 2006, **39**, 453-457.
30. F. Aquilante, J. Autschbach, R. K. Carlson, L. F. Chibotaru, M. G. Delcey, L. D. Vico, I. F. Galván, N. Ferré, L. M. Frutos, L. Gagliardi, M. Garavelli, A. Giussani, C. E. Hoyer, G. L. Manni, H. Lischka, D. Ma, P. Å. Malmqvist, T. Müller, A. Nenov, M. Olivucci, T. B. Pedersen, D. Peng, F. Plasser, B. Pritchard, M. Reiher, I. Rivalta, I. Schapiro, J. Segarra-Martí, M. Stenrup, D. G. Truhlar, L. Ungur, A. Valentini, S. Vancoillie, V. Veryazov, V. P. Vysotskiy, O. Weingart, F. Zapata and R. Lindh, *J. Comput. Chem.*, 2016, **37**, 506-541.
31. B. A. Hess, C. M. Marian, U. Wahlgren and O. Gropen, *Chem. Phys. Lett.*, 1996, **251**, 365-371.
32. B. O. Roos and P.-A. Malmqvist, *Phys. Chem. Chem. Phys.*, 2004, **6**, 2919-2927.
33. B. O. Roos, R. Lindh, P.-A. Malmqvist, V. Veryazov, P.-O. Widmark and A. C. Borin, *J. Phys. Chem. A*, 2008, **112**, 11431-11435.
34. P. A. Malmqvist, B. O. Roos and B. Schimmelpfennig, *Chem. Phys. Lett.*, 2002, **357**, 230-240.
35. L. F. Chibotaru and L. Ungur, *J. Chem. Phys.*, 2012, **137**, 064112-064122.
36. L. F. Chibotaru and L. Ungur, *POLY_ANISO program*, 2006, University of Leuven.
37. J. Long, D. M. Lyubov, T. V. Mahrova, A. V. Cherkasov, G. K. Fukin, Y. Guari, J. Larionova and A. A. Trifonov, *Dalton Trans.*, 2018, **47**, 5153-5156.
38. S. Alvarez, P. Alemany, D. Casanova, J. Cirera, M. Llunell and D. Avnir, *Coord. Chem. Rev.*, 2005, **249**, 1693-1708.
39. Y.-Z. Zhang, S. Gómez-Coca, A. J. Brown, M. R. Saber, X. Zhang and K. R. Dunbar, *Chem. Sci.*, 2016, **7**, 6519-6527.
40. S. Alvarez, *Chemical Reviews*, 2015, **115**, 13447-13483.
41. C. Benelli and D. Gatteschi, *Chem. Rev.*, 2002, **102**, 2369-2388.
42. N. F. Chilton, *CC-fit,The Univesity of Manchester, UK*, 2014, http://www.nfchilton.com/cc-fit.html.
43. K. N. Shrivastava, *Phys. stat. sol. (b)*, 1983, **117**, 437-458.
44. D. I. Alexandropoulos, K. R. Vignesh, B. S. Dolinar and K. R. Dunbar, *Polyhedron*, 2018, **151**, 255-263; K. R. Vignesh, S. K. Langley, K. S. Murray and G. Rajaraman, *Chem. Eur. J.*, 2017, **23**, 1654–1666; Y.-S. Ding, N. F. Chilton, R. E. P. Winpenny and Y.-Z. Zheng, *Angew. Chem. Int. Ed.*, 2016, **55**, 16071-16074.
45. K. R. Vignesh, S. K. Langley, K. S. Murray and G. Rajaraman, *Inorg. Chem.*, 2017, **56**, 2518-2532.
46. K. R. Vignesh, S. K. Langley, B. Moubaraki, K. S. Murray and G. Rajaraman, *Inorg. Chem.*, 2018, **57**, 1158-1170.
47. P. P. Hallmen, C. Köppl, G. Rauhut, H. Stoll and J. van Slageren, *J. Chem. Phys.*, 2017, **147**, 164101; Y. Rechkemmer, J. E. Fischer, R. Marx, M. Dörfel, P. Neugebauer, S. Horvath, M. Gysler, T. Brock-Nannestad, W. Frey, M. F. Reid and J. van Slageren, *J. Am. Chem. Soc.*, 2015, **137**, 13114-13120.
48. S. K. Langley, K. R. Vignesh, K. Holton, S. Benjamin, G. B. Hix, W. Phonsri, B. Moubaraki, K. S. Murray and G. Rajaraman, *Inorganics*, 2018, **6**.
49. M. E. Lines, *J. Chem. Phys.*, 1971, **55**, 2977-2984.
50. Y-C. Chen, J-L. Liu, W. Wernsdorfer, D. Liu, L. F. Chibotaru, X-M. Chen, and M-L. Tong, *Angew. Chem. Int. Ed.*, 2017, **56**, 4996-5000.

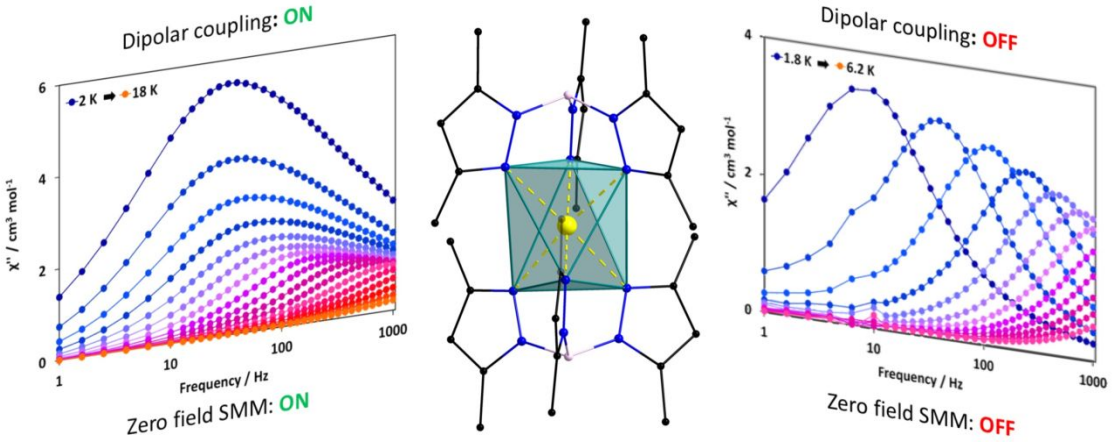

Synthesis and the detailed magnetic analysis of two new compounds containing the sandwich-type $[Dy(Tp^{Me2})_2]^+$ moiety are reported. In this cation the Dy^{III} ion is 6-coordinate, adopting a trigonally elongated octahedral geometry. Magnetic studies and *ab initio* calculations revealed that the presence or lack of intermolecular dipolar interactions has a major impact on the SMM properties of the reported compounds.